Supplementary Materials for

"Long-ranged charge order conspired by magnetism and lattice in an antiferromagnetic Kagome metal"

Ziyuan Chen[1,†], Xueliang Wu[2,†], Shiming Zhou[1,†], Jiakang Zhang[1], Ruotong Yin[1], Yuanji Li[1], Mingzhe Li[1], Jiashuo Gong[1], Mingquan He[2], Yisheng Chai[2], Xiaoyuan Zhou[2], Yilin Wang[1,3,*], Aifeng Wang[2,*], Ya-Jun Yan[1,*], Dong-Lai Feng[1,3,4,5,*]

[1] *School of Emerging Technology and Department of Physics, University of Science and Technology of China, Hefei, 230026, China*

[2] *Low temperature Physics Laboratory, College of Physics and Center of Quantum Materials and Devices, Chongqing University, Chongqing 401331, China*

[3] *National Synchrotron Radiation Laboratory and School of Nuclear Science and Technology, New Cornerstone Science Laboratory, University of Science and Technology of China, Hefei, 230026, China*

[4] *Collaborative Innovation Center of Advanced Microstructures, Nanjing, 210093, China*

[5] *Shanghai Research Center for Quantum Sciences, Shanghai, 201315, China*

1. Short-ranged charge order in sample #1

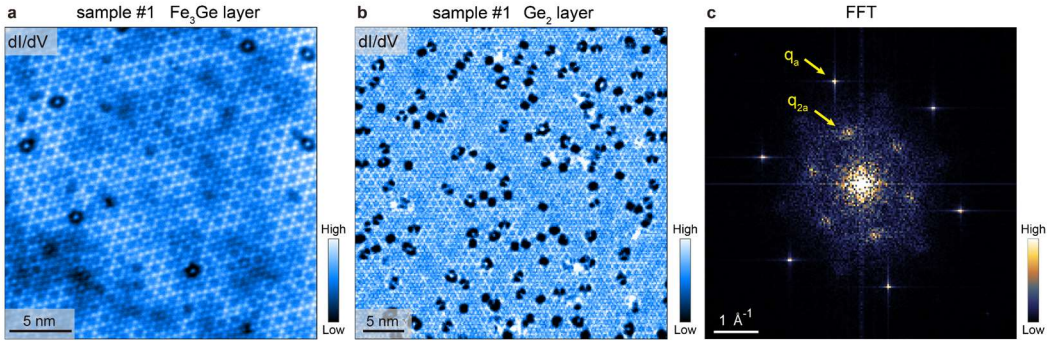

Fig. S1 | Short-ranged CO in sample #1. a,b, Typical dI/dV maps of the Fe_3Ge and Ge_2 layers of sample #1, showing a short-ranged CO in both surfaces. Panel **a** is adapted from ref. 1. **c,** FFT image of panel **a**, with the Bragg spots of underlying lattice and the CO spots labeled as q_a and q_{2a}, respectively. The q_{2a} spots are much more broadened than the q_a spots, further demonstrating the short-ranged behavior of the CO in sample #1. Measurement conditions: **a,** V_b = 0.3 V, I_t = 300 pA, ΔV = 30 mV; **b,** V_b = 0.4 V, I_t = 200 pA, ΔV = 5 mV.

2. Density of defects in more sample regions of samples #1 and #2

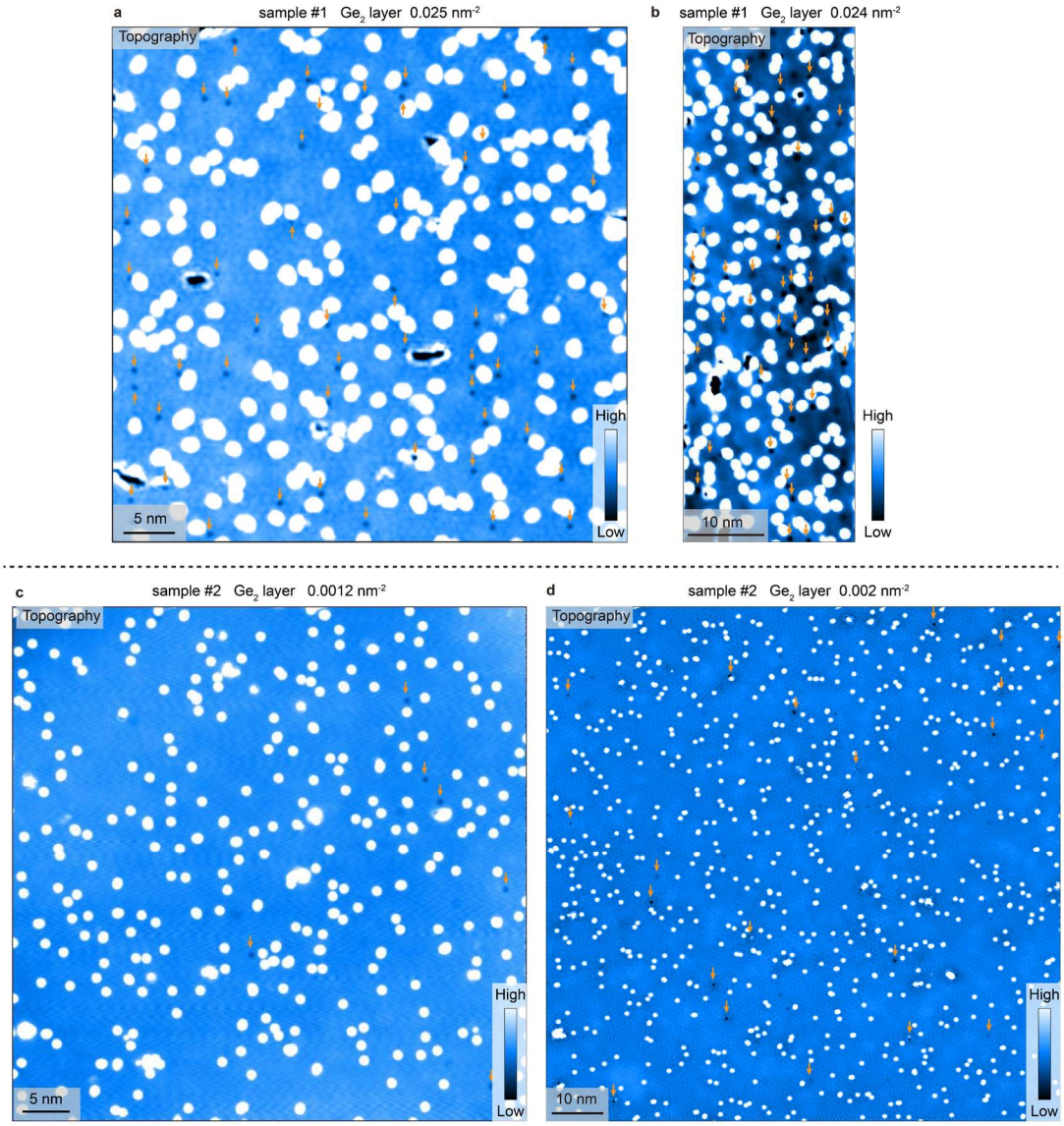

Fig. S2 | More datasets for defect distribution in the Ge_2 layers of samples #1 and #2. a,b, Typical topographic images of Ge_2 layer in sample #1. **c,d,** Typical topographic images of Ge_2 layer in sample #2. The native defects are indicated by the orange arrows and their total densities are shown. Measurement conditions: **a,b,** V_b = 1.0 V, I_t = 10 pA; **c,** V_b = 1.0 V, I_t = 100 pA; **d,** V_b = 12 mV, I_t = 300 pA.

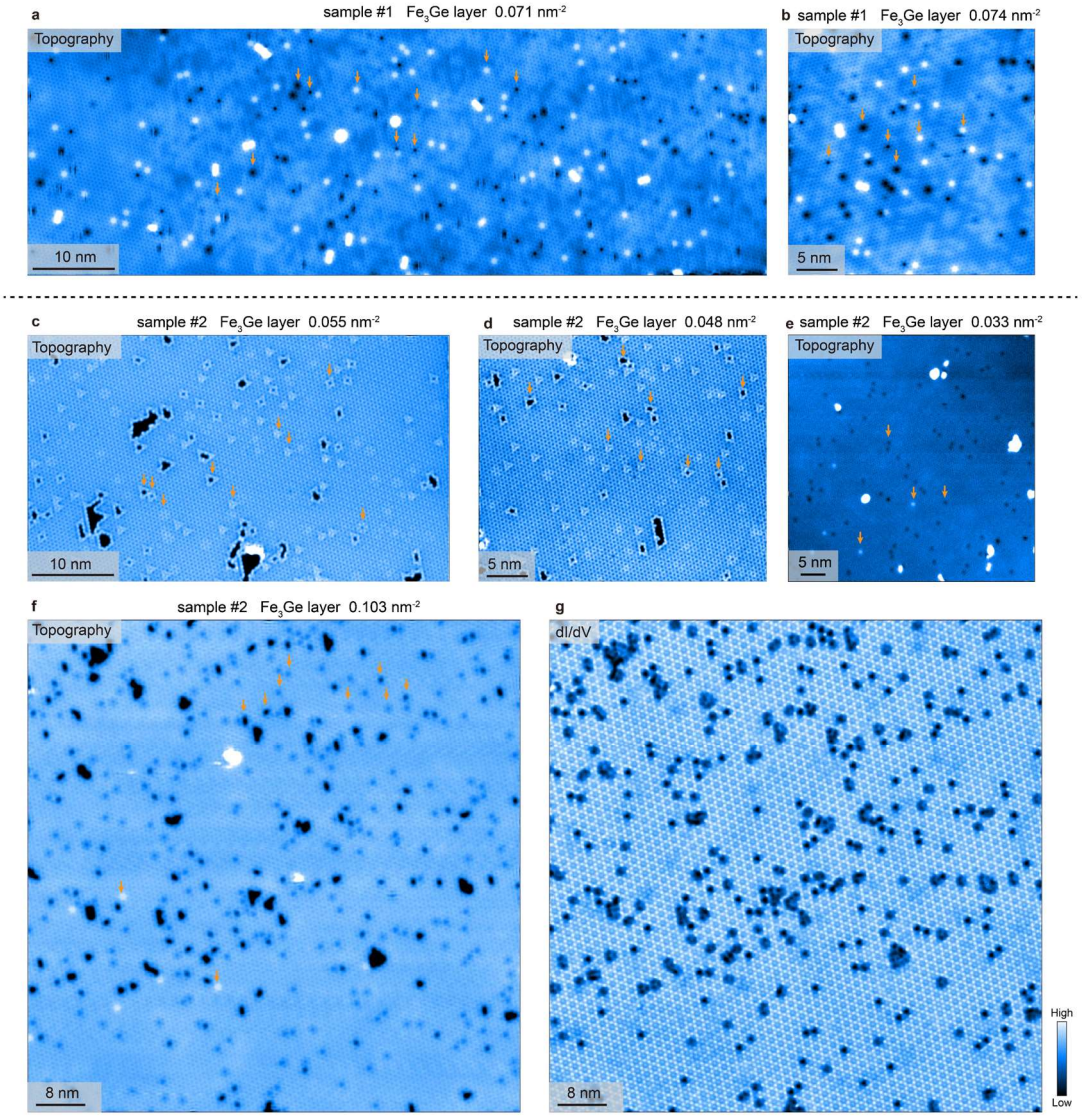

Fig. S3 | More datasets for defect distribution in the Fe_3Ge layers of samples #1 and #2. a,b, Typical topographic images of Fe_3Ge layer in sample #1. **c-f**, Typical topographic images of Fe_3Ge layer in sample #2. **g**, dI/dV map in the region shown in panel **f**, exhibiting a long-ranged CO. Partial native defects are indicated by the orange arrows and the total densities of defects are shown. Measurement conditions: **a**, V_b = 1.0 V, I_t = 20 pA; **b**, V_b = 1.0 V, I_t = 10 pA; **c**,**d**, V_b = -40 mV, I_t = 300 pA; **e**, V_b = 1.0 V, I_t = 50 pA; **f**, V_b = 1.0 V, I_t = 300 pA; **g**, V_b = 0.2 V, I_t = 300 pA, ΔV = 20 mV.

3. More datasets for the long-ranged 2 × 2 × 2 CO in sample #2

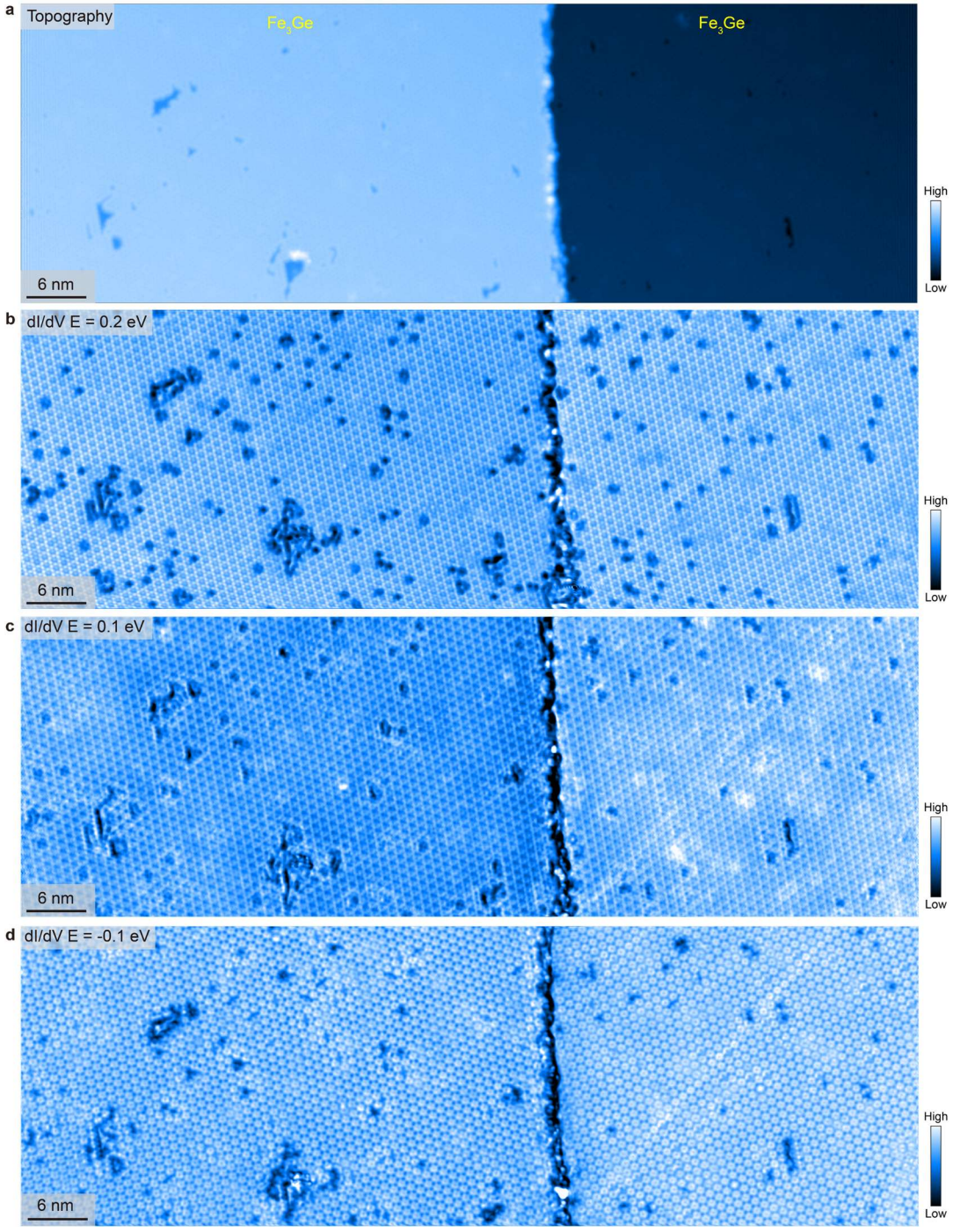

Fig. S4 | Topographic image and more d*I*/d*V* maps under various energies for a Fe_3Ge region. A long-ranged CO is obvious for all the maps, although the detailed CO patterns vary with energy. Measurement conditions: **a,** V_b = 0.3 V, I_t = 300 pA; **b**, V_b = 0.2 V, I_t = 300 pA, ΔV = 20 mV; **c,** V_b = 0.1 V, I_t = 300 pA, ΔV = 20 mV; **d,** V_b = -0.1 V, I_t = 300 pA, ΔV = 20 mV.

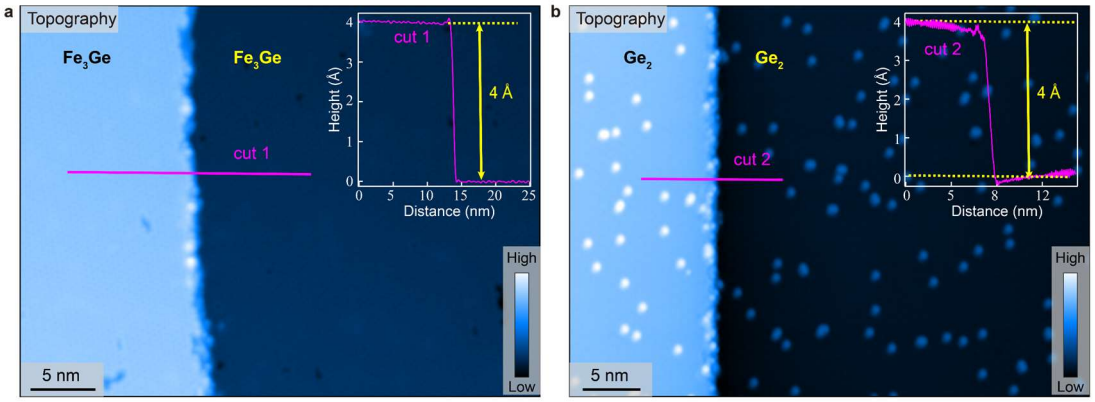

Fig. S5 | Topographic images of Fig. 2a,b. Insets: height profiles obtained along the magenta lines shown in panels **a**,**b**. The heights of the Fe_3Ge-Fe_3Ge and Ge_2-Ge_2 single-unit-cell-height steps are ~ 4 Å. Measurement conditions: **a,** V_b = 0.3 V, I_t = 300 pA; **b,** V_b = 0.2 V, I_t = 300 pA.

4. Detailed SCXRD results for samples #1 and #2

SCXRD measurements were carried out on both samples #1 and #2 at 300 K and 85 K, respectively. The diffraction patterns of these two samples are the same at 300 K, but vary significantly at 85 K, as displayed in Fig. 3, S6 and S7. At 85 K, new spots are observed for sample #2 and signal a structural modulation with a wave vector of (-0.5, 0.5, 0.5), while they are absent in sample #1. By using Olex2 software with Shlex program[2,3], the corresponding crystal structures are solved and refined, as shown in Tables S1-S6 and Fig. S8. For both samples at 300 K, high quality refinements are achieved with the space group P6/*mmm*. The refined atomic coordinates are listed in Tables S2 and S5, and the corresponding crystal structure is sketched in Fig. 3**c** and S8**a-d**, which is consistent with the previous report[4]. The same space group and atomic coordinates can also describe the diffraction patterns of sample #1 at 85 K (Table S3). However, for the diffraction patterns of sample #2 at 85 K, a higher quality refinement is achieved with the space group P-6*m*2. The P-6*m*2 unit cell presented in Table S4 is eight times larger than the primitive unit cell at 300 K, with the lattice doubling along all three lattice directions. The related atomic coordinates are listed in Table S6, and the corresponding crystal structure is sketched in Fig. 3**d** and S8**e-h**. The largest distortion occurs at the Ge1a sites in the Kagome layers, where the Ge1a atoms in the adjacent two layers dimerize and deviate from the Kagome layer by ~ 0.7 Å. Other atoms in the Kagome layer also undergo small distortions (< 5 pm), and are out-of-phase between adjacent Kagome layers. Ge1b atoms mainly distort along the *c*-axis, the Fe atoms are distorted both within the plane and along the *c*-axis. The distortion of Ge_2 layer is simpler, showing a deformed Kekulé-type distortion and is out-of-phase between adjacent Ge_2 layers.

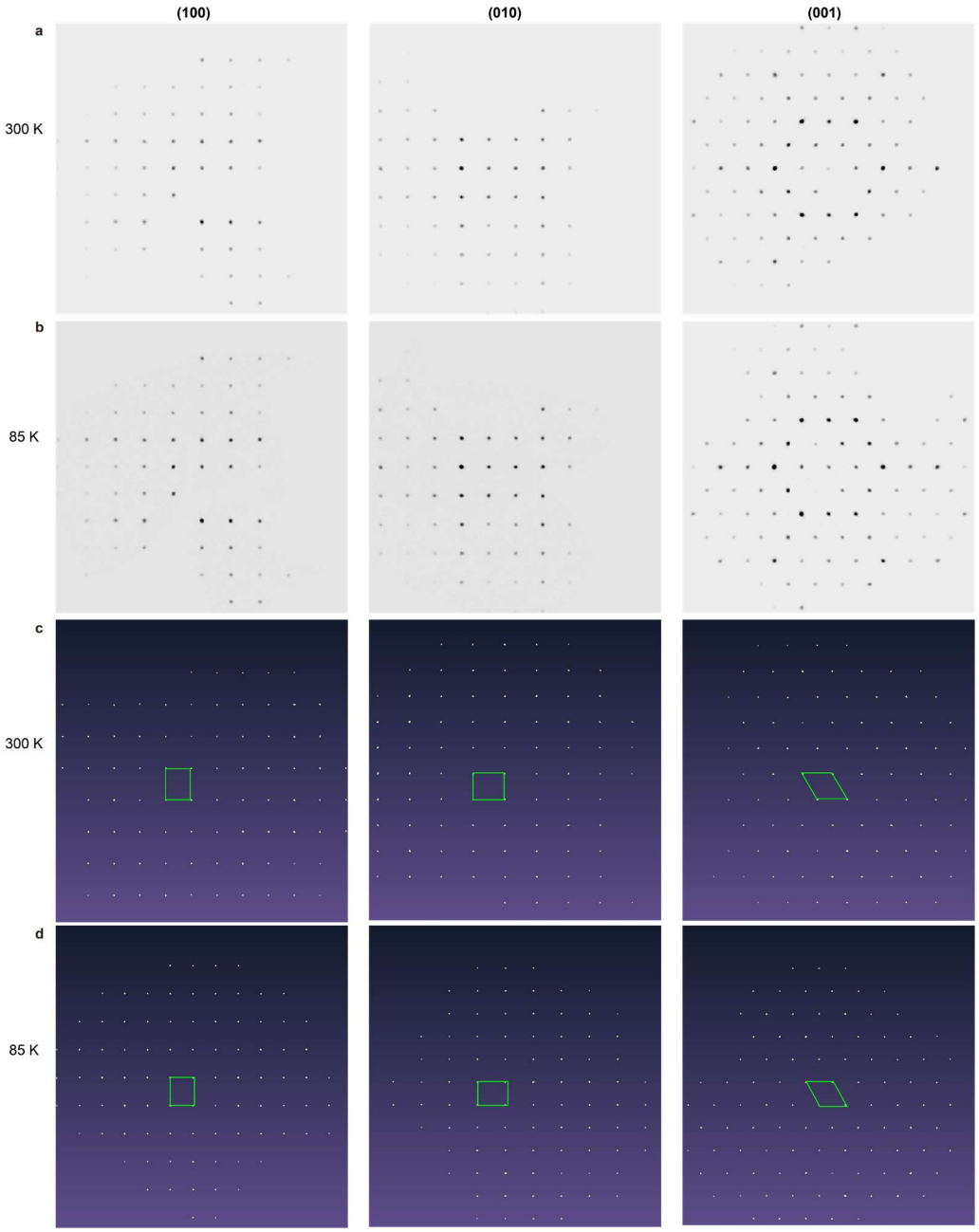

Fig. S6 | Diffraction patterns (a and b) and lattice peaks (c and d) along the *a*-, *b*- and *c*-axes for sample #1, measured at 300 K and 85 K, respectively. Unit cells are indicated by the green rectangular and rhombic boxes. There are no obvious superstructure spots appeared at 85 K.

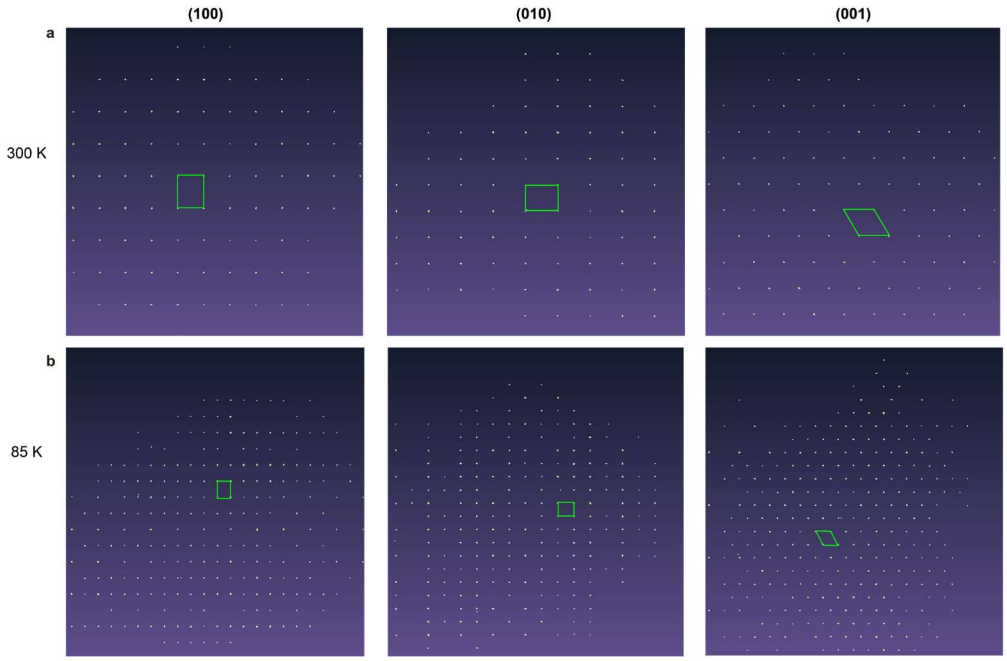

Fig. S7 | Lattice peaks along the *a*-, *b*-, and *c*-axes for sample #2 measured at 300 K and 85 K, respectively. Unit cells are indicated by the green rectangular and rhombic boxes. New spots appear at 85 K, signaling that the lattice doubles along all three lattice directions.

Table S1. Crystal data and structure refinement for sample #1 at 300 and 85 K.

Temperature/K	300	85
Empirical formula	FeGe	FeGe
Formula weight	128.44	128.44
Crystal system	hexagonal	hexagonal
Space group	P6/mmm	P6/mmm
a/Å	4.9956(8)	4.9859(4)
b/Å	4.9956(8)	4.9859(4)
c/Å	4.0606(7)	4.0471(4)
α/°	90	90
β/°	90	90
γ/°	120	120
Volume/Å^3	87.76(3)	87.131(17)
Z	3	3
ρ_{calc}g/cm^3	7.291	7.343
μ/mm^{-1}	37.158	37.426
F(000)	174	174
Crystal size/mm^3	0.16 × 0.14 × 0.14	0.16 × 0.14 × 0.14
Radiation	Mo Kα (λ = 0.71073)	Mo Kα (λ = 0.71073)
2Θ range for data collection/°	9.424 to 58.64	9.442 to 58.496
Index ranges	-6 ≤ h ≤ 5, -4 ≤ k ≤ 6, -5 ≤ l ≤ 4	-6 ≤ h ≤ 6, -6 ≤ k ≤ 6, -4 ≤ l ≤ 5
Reflections collected	505	591
Independent reflections	68 [R_{int} = 0.0335, R_{sigma} = 0.0218]	67 [R_{int} = 0.0408, R_{sigma} = 0.0200]
Data/restraints/parameters	68/0/8	67/0/9
Goodness-of-fit on F^2	1.154	1.213
Final R indexes [I>=2σ (I)]	R_1 = 0.0359, wR_2 = 0.0923	R_1 = 0.0569, wR_2 = 0.1371
Final R indexes [all data]	R_1 = 0.0359, wR_2 = 0.0923	R_1 = 0.0569, wR_2 = 0.1371
Largest diff. peak/hole / e Å^{-3}	3.97/-1.75	9.64/-4.79

Table S2. Refined atomic coordinates and equivalent isotropic displacement (U_{eq}) parameters for sample #1 at 300 K.

Atom	*x*	*y*	*z*	U_{eq}	Occ.
Ge1	2/3	1/3	1/2	0.007	1.0
Ge2	0	0	0	0.012	1.0
Fe1	1/2	1/2	0	0.006	1.0

Table S3. Refined atomic coordinates and equivalent isotropic displacement (U_{eq}) parameters for sample #1 at 85 K.

Atom	*x*	*y*	*z*	U_{eq}	Occ.
Ge1	2/3	1/3	1/2	-0.003	1.0
Ge2	0	0	0	0.011	1.0
Fe1	1/2	1/2	0	-0.001	1.0

Table S4. Crystal data and structure refinement for sample #2 at 300 and 85 K.

Temperature/K	300	85
Empirical formula	FeGe	FeGe
Formula weight	128.44	128.44
Crystal system	hexagonal	hexagonal
Space group	P6/mmm	P-6m2
a/Å	4.9948(6)	9.9552(8)
b/Å	4.9948(6)	9.9552(8)
c/Å	4.0534(5)	8.0817(7)
α/°	90	90
β/°	90	90
γ/°	120	120
Volume/Å^3	87.57(2)	693.64(13)
Z	3	24
ρ_{calc}g/cm^3	7.306	7.379
μ/mm^{-1}	37.237	37.610
F(000)	174.0	1392.0
Crystal size/mm^3	0.08 × 0.07 × 0.14	0.08 × 0.07 × 0.14
Radiation	Mo Kα (λ = 0.71073)	Mo Kα (λ = 0.71073)
2Θ range for data collection/°	9.424 to 58.664	6.91 to 58.65
Index ranges	-6 ≤ h ≤ 6, -6 ≤ k ≤ 6, -5 ≤ l ≤ 5	-11 ≤ h ≤ 12, -12 ≤ k ≤ 13, -10 ≤ l ≤ 9
Reflections collected	607	3493
Independent reflections	69 [R_{int} = 0.0329, R_{sigma} = 0.0158]	705 [R_{int} = 0.0256, R_{sigma} = 0.0206]
Data/restraints/parameters	69/0/9	705/0/55
Goodness-of-fit on F^2	1.278	1.092
Final R indexes [I>=2σ (I)]	R_1 = 0.0180, wR_2 = 0.0388	R_1 = 0.0317, wR_2 = 0.0724
Final R indexes [all data]	R_1 = 0.0180, wR_2 = 0.0388	R_1 = 0.0385, wR_2 = 0.0777
Largest diff. peak/hole / e Å^{-3}	2.29/-1.20	3.38/-1.68

Table S5. Refined atomic coordinates and equivalent isotropic displacement (U_{eq}) parameters for sample #2 at 300 K.

Atom	*x*	*y*	*z*	U_{eq}	Occ.
Ge1	2/3	1/3	1/2	0.007	1.0
Ge2	0	0	0	0.011	1.0
Fe1	1/2	1/2	0	0.006	1.0

Table S6. Refined atomic coordinates and equivalent isotropic displacement (U_{eq}) parameters for sample #2 at 85 K.

Atom	x	*y*	*z*	Ueq	Occ.
Ge1a	2/3	1/3	0.1656	0.006	1
Ge1b	0.1666	0.3332	0.2526	0.003	1
Fe1a	0.1661	0.0830	0.2530	0.001	1
Fe1b	0.4161	0.3343	0.2469	0.002	1
Fe1c	0.4171	0.5829	0.2530	0.002	1
Ge2a	0	0	1/2	-0.002	1
Ge2b	1/3	2/3	1/2	0.005	1
Ge2c	0.3440	0.1720	1/2	0.006	1
Ge2d	0.5043	0.4957	1/2	-0.002	1
Ge2e	0	0	0	-0.003	1
Ge2f	1/3	2/3	0	0.007	1
Ge2g	0.3268	0.1634	0	0.006	1
Ge2h	0.4967	0.5032	0	-0.003	1

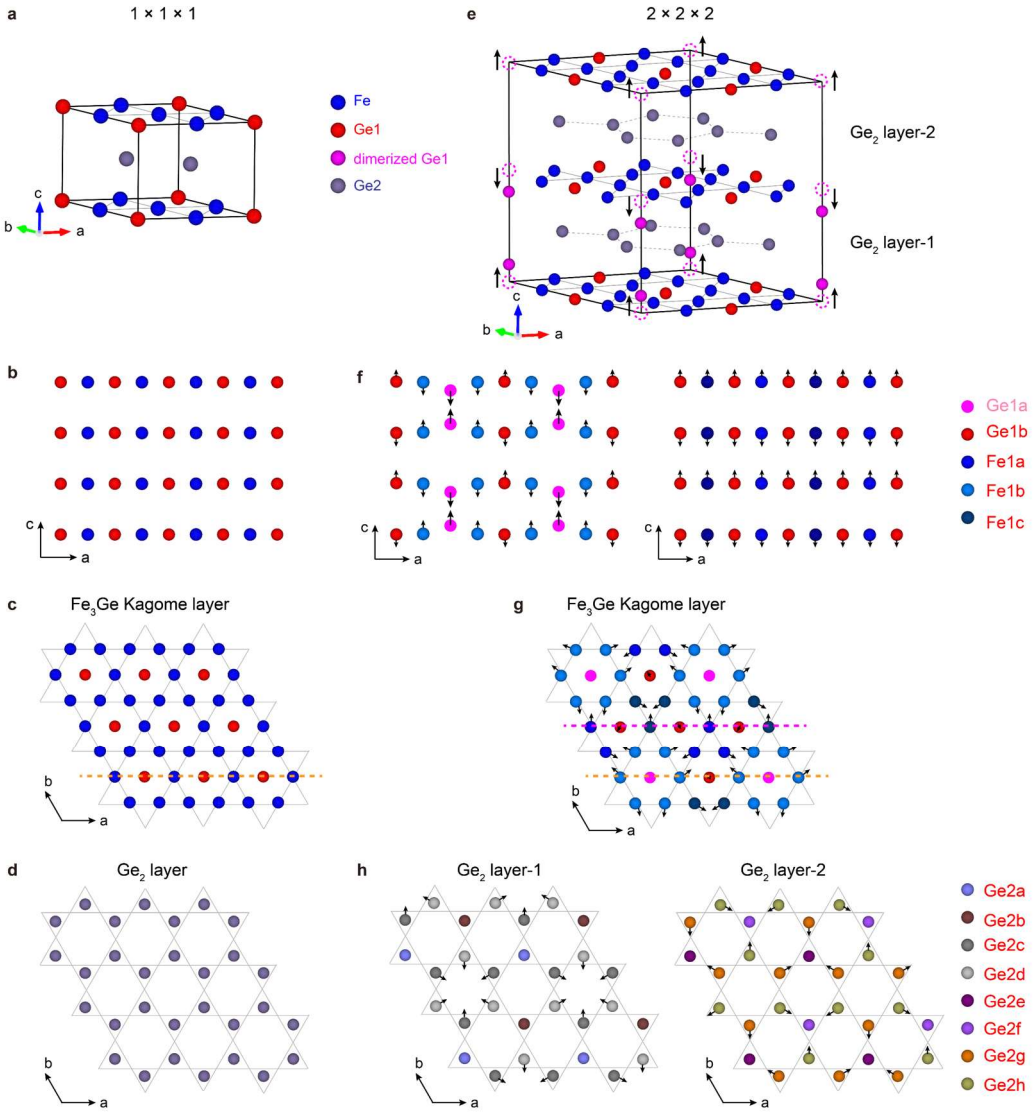

Fig. S8 | Detailed lattice distortion of the CO superstructure. a-d, Lattice structure of FeGe at 300 K. Panel **b** shows the projection of (010) plane along the direction indicated by the orange dashed line in panel **c**. **e-h**, Detailed lattice structure of the CO superstructure measured at 85 K. Panel **f** shows the projections of (010) planes along the directions indicated by the orange and magenta dashed lines in panel **g**, exhibiting atomic distortions along the *c*-axis. **g,h,** In-plane atomic distortions in the Fe_3Ge and Ge_2 layers. The black arrows indicate the direction and magnitude of atom distortion.

5. More datasets for CO disruption

Figure S9 shows the details of the 2 × 2 × 2 CO (Fig. S9**a-d**) and the 1 × 1 × 1 phase (Fig. S9**e-h**) obtained after CO disruption. By repeating the CO disruption process, the 2 × 2 × 2 CO disappears completely, leaving a pure 1 × 1 × 1 phase, as reflected more clearly in the FFT images (Fig. S9**f** and S9**h**). Moreover, we have measured the topographic images of several phase separation regions in both the Fe_3Ge and Ge_2 layers under various energies, as shown in Fig. S10. We find that in all cases, the lattice of the 1 × 1 × 1 phase is slightly higher by 6-7 pm than that of the 2 × 2 × 2 CO phase.

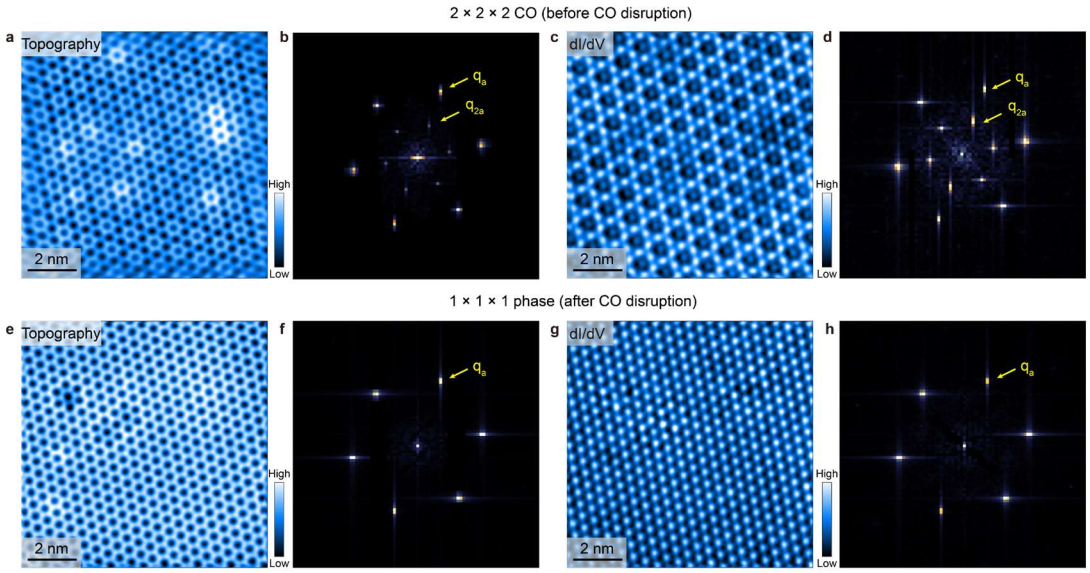

Fig. S9 | Details of the 2 × 2 × 2 CO and the 1 × 1 × 1 phase obtained after CO disruption. a-d, Typical topographic image, dI/dV map and corresponding FFT images of a selected Fe_3Ge region before CO disruption. **e-h,** Typical topographic image, dI/dV map and corresponding FFT images of the same Fe_3Ge region after CO disruption. The 2 × 2 × 2 CO disappears completely after CO disruption, leaving a pure 1 × 1 × 1 phase. Measurement conditions: **a,e,** V_b = 0.2 V, I_t = 300 pA; **c,g,** V_b = 0.2 V, I_t = 300 pA, ΔV = 30 mV.

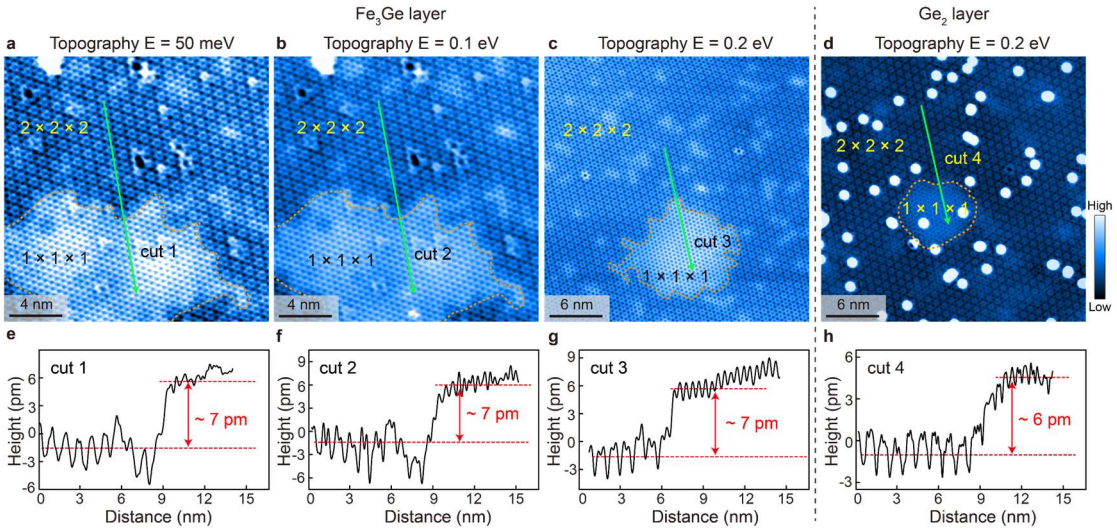

Fig. S10 | Height difference between the 2 × 2 × 2 CO and the 1 × 1 × 1 phase in both the Fe_3Ge and Ge_2 layers. a-c, Typical topographic images of the phase separation regions in Fe_3Ge layer, measured under different energies. **d,** Typical topographic image of the phase separation region in Ge_2 layer. **e-h,** Lattice line profiles taken along cuts 1-4, as indicated in panels **a-d**. A height difference of 6-7 pm is obtained for all the cases. Measurement conditions: **a,** V_b = 50 mV, I_t = 300 pA; **b,** V_b = 0.1 V, I_t = 300 pA; **c,d,** V_b = 0.2 V, I_t = 300 pA.

Supplementary References:

1. Chen, Z. Y. et al. Charge density wave with strong quantum phase fluctuations in Kagome magnet FeGe. ArXiv: 2302.04490 (2023).
2. Dolomanov, O.V. et al. OLEX2: a complete structure solution, refinement and analysis program. *J. Appl. Cryst.* **42**, 339 (2009).
3. Sheldrick, G. M. A short history of SHELX. *Acta Cryst.* **A64**, 112 (2008).
4. Teng, X. K. et al. Discovery of charge density wave in a kagome lattice antiferromagnet. *Nature* **609**, 490 (2022).